

Low-Temperature Magnetism in the Honeycomb Systems SrLn_2O_4

O.A. Petrenko

University of Warwick, Department of Physics, Coventry, CV4 7AL, UK

(Dated: March 5, 2014)

Recent progress in the understanding of the complex magnetic properties of the family of rare-earth strontium oxides, SrLn_2O_4 , is reviewed. These compounds consisting of hexagons and triangles are affected by geometrical frustration and therefore exhibit its characteristic features, such as a significant reduction of magnetic ordering temperatures and complex phase diagrams in an applied field. Some of the observed features appear to be rather remarkable even in the context of the unusual behaviour associated in geometrically frustrated magnetic systems. Of particular interest is the coexistence at the lowest temperature of different magnetic structures (exhibiting either long or short-range order) characterised by different propagation vectors in materials without significant chemical or structural disorder.

PACS numbers: 75.25.-j, 75.50.Ee, 75.47.Lx

I. INTRODUCTION

Frustrated magnets have been a focal point of the research on magnetism for the past two decades. In this article, the influence of geometrical frustration on the magnetic properties of the family of rare-earth strontium oxides, SrLn_2O_4 , (where $\text{Ln} = \text{Gd}, \text{Dy}, \text{Ho}, \text{Er}, \text{Tm}, \text{and Yb}$) is discussed. Given the nature of this special issue of *Low Temperature Physics* on antiferromagnetism an extensive general introduction to magnetically frustrated systems is omitted and the reader is instead referred to a collection of reviews available on the subject¹. We start with a description of the crystal structure and general properties of SrLn_2O_4 and other closely related compounds and then present the recently obtained experimental results on their low-temperature magnetic properties by our group and others. Particular attention is paid to the zero-field ground state of SrEr_2O_4 , SrHo_2O_4 , and SrDy_2O_4 (section II), as well as the field-induced behaviour of these compounds (section III). The penultimate section briefly reviews the other SrLn_2O_4 compounds and discusses the importance of crystal field effects. The concluding section compares different members of the family and includes a brief summary.

The members of the SrLn_2O_4 family crystallise in the form of calcium ferrite², with the space group $Pnam$; the crystal structure of these materials (see Fig. 1) can be viewed as a network of linked hexagons and triangles^{3,4}. The most important feature of the linked hexagon (or “honeycomb”) lattice is that it has the lowest coordination number, 3, in two dimensions. This feature attracts a lot of theoretical attention to the lattice, but being bipartite, the honeycomb lattice is not frustrated if only the nearest-neighbour interactions are considered. The frustration in a honeycomb lattice can be induced by further neighbour interaction and numerous models of frustrated honeycomb lattices which include Heisenberg, XY or Ising $J_1 - J_2 - J_3$ interactions have been extensively studied theoretically, particularly for the $s = 1/2$ quantum case.

In the SrLn_2O_4 family, however, the cause of frustra-

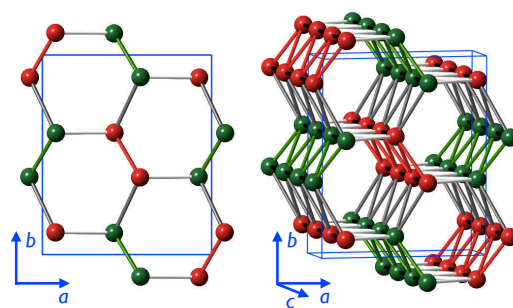


FIG. 1: Positions of the magnetic rare-earth Ln^{3+} ions within the SrLn_2O_4 compounds, with the two crystallographically inequivalent Ln^{3+} sites shown in different colours. The left-hand panel emphasises the honeycomb arrangement of the Ln^{3+} ions when viewed along the c axis, while the right-hand panel demonstrates the formation of zigzag ladders running along the c axis which link the honeycomb layers and give rise to geometric frustration. The blue box represents a crystal unit cell of the $Pnam$ space group.

tion is different; it arises from the triangular (or “zigzag”) ladders running along the c axis which link the honeycomb layers. In this respect SrLn_2O_4 compounds are similar to recently reported $\beta - \text{CaCr}_2\text{O}_4$ ⁵ and perhaps to LnV_4O_8 compounds⁶. The term “zigzag” has also been used to describe the spin-chain structure of another honeycomb lattice compound Na_2IrO_3 ^{7,8}, but in a different context - to describe the arrangement of magnetic moments formed there.

The orthorhombic unit cell of the SrLn_2O_4 compounds contains 4 Sr atoms on a single site, 8 Ln atoms (split equally between two sites) and 16 oxygen atoms occupying 4 sites; all sites are of the $4c$ type with the coordinates $(x, y, 1/4)$ ⁴. The a and b axes of the unit cell are typically quite long, about 10 and 12 Å respectively, while the c axis is the shortest, at around 3.4 Å on average. The magnetic Ln atoms are surrounded by the distorted oxygen octahedra, forming the chains running along the c -axis. The shortest $\text{Ln} - \text{Ln}$ separation is along the

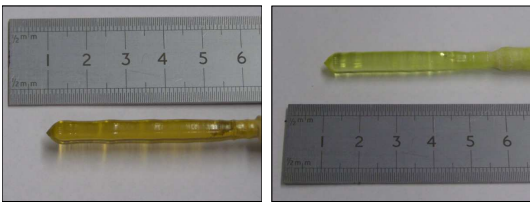


FIG. 2: As grown boules of SrHo_2O_4 (left panel) and SrDy_2O_4 (right panel) single crystals, using growth speeds of 6 to 8 mm/h. Figure is from Ref.¹⁰.

chains; there is a slightly larger separation between the chains formed by the Ln atoms occupying the same sites (which are shown in Fig. 1 in the same colour), while the distance between Ln atoms from different sites (red and green in Fig. 1) is much greater⁴. Such a crystal structure predetermines the quasi one-dimensional magnetic properties of the SrLn_2O_4 compounds, as for rare-earth ions in insulating materials direct exchange is often the most important mechanism for magnetic coupling. It is rather useful to note the equivalence of the well-studied linear chain model with nearest and next-nearest interactions⁹ and the ladders of rare-earth ions described here if these were “stretched” along the c axis.

An important observation to make prior to the description of their properties is that both polycrystalline and single crystal samples of the SrLn_2O_4 compounds have been used for investigations. The progress achieved to date in the understanding of their complex behaviour is, however, largely due to the availability of high quality single crystals. Crystals of magnetic SrLn_2O_4 oxides and their non-magnetic analogues (with $\text{Ln} = \text{Lu}$ or Y) have been synthesised by the floating zone technique by our group and others^{10–12}. Examples of the single crystals grown¹⁰ are shown in Fig. 2; the size of the crystals available is certainly sufficient for neutron scattering experiments, including inelastic studies. In comparison, the magnetic properties of structurally similar BaLn_2O_4 (Ref. 13), EuLn_2O_4 (Ref. 14,15) and $\text{Ba}_2\text{Ln}_2\text{S}_4$ (Ref. 16) compounds have not yet been probed to a significant degree, as only polycrystalline samples are available.

II. ZERO FIELD MAGNETIC PROPERTIES OF SrEr_2O_4 , SrHo_2O_4 AND SrDy_2O_4

A. SrEr_2O_4

SrEr_2O_4 is found to order magnetically at $T_N = 0.75$ K with a $\mathbf{k} = 0$ antiferromagnetic (AFM) structure (depicted in Fig. 3) consisting of ferromagnetic chains running along the c axis, with adjacent chains arranged antiferromagnetically¹⁷. The refinement of the powder neutron diffraction (PND) data suggested that the moments point along the c direction and that only one of the

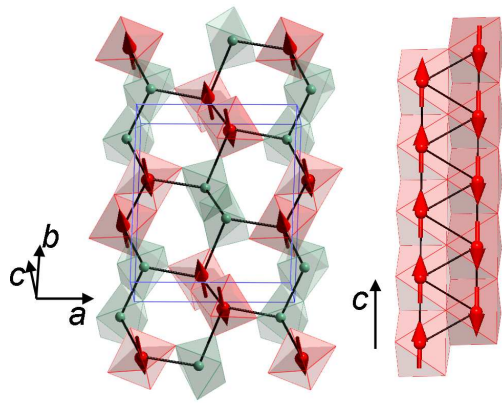


FIG. 3: Magnetic structure of SrEr_2O_4 as determined from Rietveld refinements of the neutron-diffraction pattern at $T = 0.55$ K. The same structure is shown twice to emphasise different arrangements of the magnetic moments along the c axis and with respect to the hexagons in the plane. Two different Er sites and their surroundings are shown in different colours. Only one of the sites carries a significant magnetic moment. Figure is from Ref. [17].

two Er^{3+} sites possesses a sizeable magnetic moment. It was not possible to determine which particular site contributed to the ordering, as the magnetic moments may be swapped between the two sites without changing the calculated PND pattern significantly¹⁷.

The situation with the low-temperature magnetic structure of SrEr_2O_4 became much clearer after the publication of single crystal polarised neutron diffraction results¹⁸, which are summarised in Fig. 4. The presence of a magnetic component with long-range order (LRO) below 0.75 K was confirmed by the observation of sharp resolution-limited Bragg peaks at integer (hkl) positions (see Fig. 4a). These peaks are replaced by broad and much weaker diffuse scattering features above T_N (see Fig. 4b). Surprisingly, another distinct magnetic component corresponding to a short-range incommensurate structure was also detected. This component manifests itself by the presence of a strong diffuse signal, forming the undulated planes of scattering, which are seen as “rods” in a particular scattering plane. Fig. 4c, for example, clearly shows the two rods are at positions $(0, k, 1/2 + \delta)$ and $(0, k, 3/2 - \delta)$, where δ is dependent upon k . A Monte Carlo simulation¹⁸ showed that a simple model based on a ladder of triangles in which the nearest-neighbour interactions are approximately five times stronger than the next-nearest-neighbour interactions satisfactorily mimics the observed diffuse scattering patterns.

From the width of the diffuse “rods” at the base temperature, the estimates for correlation length along the c axis vary from 130 to 70 Å depending on which “rod” is considered¹⁸, but in any event the AFM correlations are rather long and include more than 20 magnetic ions. The interpretation of these data is that apart from the $\mathbf{k} = 0$

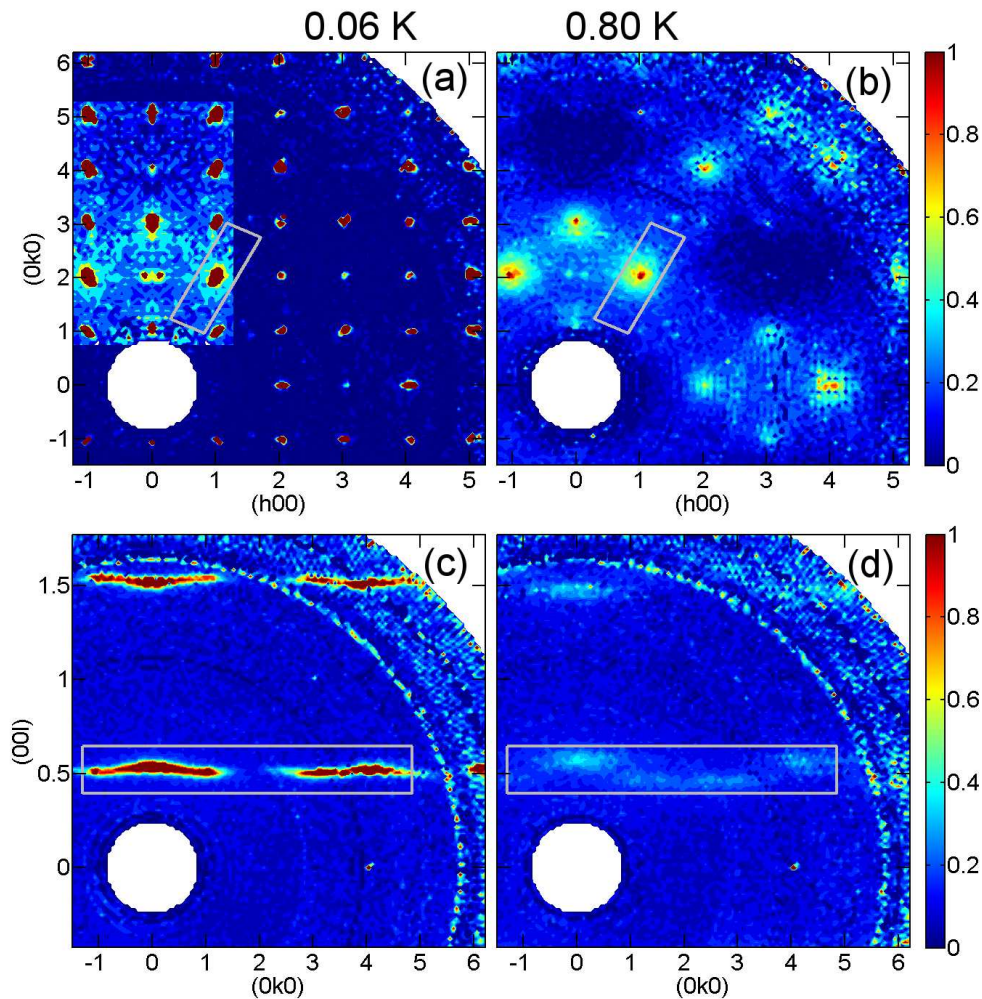


FIG. 4: Reciprocal space intensity maps of the magnetic scattering from SrEr_2O_4 in the $(hk0)$ plane (top panels) and in the $(0kl)$ plane (bottom panels) at 0.06 K (left panels) and 0.8 K (right panels). The highlighted area $1.3 < h < 1.3$, $0.7 < k < 5.3$ in panel (a) has 10 times lower intensity scale to emphasise the presence at the lowest temperature of a weak diffuse scattering otherwise obscured by the much more intense Bragg peaks. The magnetic scattering is isolated from the nuclear and spin-incoherent contribution by full XYZ polarisation analysis using D7 diffractometer for the $(hk0)$ plane. In the case of maps of the $(0kl)$ plane, the intensity shown is obtained by removing the nuclear contribution from the non-spin-flip measurement with neutrons polarised orthogonal to the scattering plane, following Ref.²¹. Figure is from Ref. [18].

LRO component shown in Fig. 3) the magnetic structure of SrEr_2O_4 consists of highly correlated AFM chains running along the c axis, but the correlations between the chains are rather weak.

On warming from the base temperature of a dilution cryostat to much higher temperatures, the partially ordered component does not undergo a pronounced phase transition unlike the $\mathbf{k} = 0$ component. Instead it gradually loses the intensity, but it could be easily seen at 0.8 K (see Fig. 4d) and in fact much higher temperatures (not shown).

From the polarisation analysis¹⁸, the magnetic moments in the long-range commensurate and short-range incommensurate structures are found to be predominantly pointing along the c and a axes, respectively.

B. SrHo_2O_4

At a first glance, a refinement of the low-temperature magnetic structure of SrHo_2O_4 looks very similar to SrEr_2O_4 . The PND data¹⁹ returned a collinear AFM $\mathbf{k} = 0$ component, very similar to the one shown in Fig. 3, below the ordering temperature of 0.68 K, with only a half of the Ho^{3+} ions carrying a significant moment. The presence of another magnetic component was also observed as a pronounced scattering around the $(0, 0, 1/2)$ positions. Further single crystal diffraction data²⁰, however, revealed a more complicated picture.

The observed broad diffraction peaks show that the $\mathbf{k} = 0$ component (corresponding to a collinear antiferromagnetically coupled structure) is of short-range order

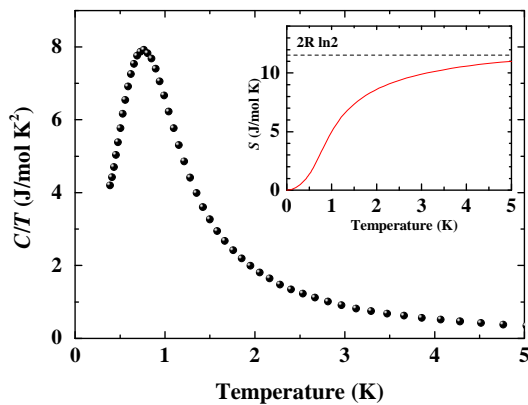


FIG. 5: Temperature dependence of the specific heat divided by temperature of SrDy_2O_4 in zero field. The inset shows the temperature dependence of the entropy, S (solid line), calculated as the area under the $C(T)/T$ curve which has been extended linearly down to $T = 0$ K. The dashed line indicates the position of $2R\ln(2)$, which corresponds to the magnetic contribution for a system with an effective $s = 1/2$. Figure is from Ref. [22].

type. The planes of diffuse scattering corresponding to another kind of magnetic order appear to be nearly perfectly commensurate, *i.e.* the parameter δ is almost zero for them, although the variations of the intensity have been seen in both the $(h0l)$ and $(0kl)$ planes in reciprocal space. This observation suggests that the second type of short-range order present in SrHo_2O_4 is principally one-dimensional in nature, that is the magnetic structure is essentially a collection of AFM coupled chains running along the c axis with the intrachain correlations remaining rather weak down to lowest temperatures. Similarly to what have been observed in SrEr_2O_4 , a magnetic component with the propagation vector $\mathbf{k} = 0$ exists below a well-defined transition temperature, while the one-dimensional scattering is observed at much higher temperatures.

Correlation lengths associated with the broad peaks are about 150 \AA in the ab plane and about 190 \AA along the c axis, while the correlation length associated with the diffuse scattering planes is 230 \AA along the c axis at the lowest temperature. From the polarisation analysis²⁰, the magnetic moments in the $\mathbf{k} = 0$ and quasi one-dimensional structures are found to be pointing along the c and b axes, respectively.

C. SrDy_2O_4

In contrast to the other members of the SrLn_2O_4 family investigated so far, SrDy_2O_4 does not show any sign of magnetic phase transition down to the lowest available temperatures. In zero field, heat capacity $C(T)$ measurements indicate that this compound appears to be magnetically disordered down to at least 0.39 K (see

Fig. 5). The $C(T)/T$ curve shows a very broad maximum at 0.77 K and a nearly linear temperature dependence below this peak. There are no sharp features in the heat capacity curve which can be attributed to a phase transition to a magnetically ordered state. PND data for SrDy_2O_4 show no signs of any long-range magnetic order down to 20 mK , as the scattering pattern in zero field is dominated by broad diffuse scattering peaks²⁴.

The magnetic entropy recovered in SrDy_2O_4 between zero temperature and $T = 5 \text{ K}$ (see inset in Fig. 5) amounts to $2R\ln 2$, which suggests that at the lowest temperature the system is essentially a doublet with the magnetic moments restricted to point only along the easy axis (Ising) direction.

III. FIELD-INDUCED BEHAVIOUR OF SrEr_2O_4 , SrHo_2O_4 AND SrDy_2O_4

The higher-temperature magnetisation curves for the polycrystalline samples of these compounds have been reported by Karunadasa *et al.*⁴ and revealed non-linear behaviour of magnetisation in field with pronounced maxima in the derivatives, dM/dH as a function of applied field. Further single crystal magnetisation²³ and heat capacity²² measurements, however, revealed highly anisotropic behaviour, which is partially masked in the polycrystalline samples. We therefore summarise in this section the results obtained on single crystal samples.

Magnetisation versus field curves $M(H)$ and their field derivatives dM/dH obtained for SrHo_2O_4 for a field applied along the principal symmetry axes are shown in Fig. 6. For $H \parallel a$ (which is a hard magnetisation direction), $M(H)$ remains rather small in any field. For other two directions of an applied field, a significant portion of the total magnetic moment is recovered, although no complete saturation of magnetisation is observed, as the dM/dH values remain nonzero even in a field of 70 kOe ²³. This implies that the spins of the Ho^{3+} ions are not fully aligned at this field. For $H \parallel b$ the magnetisation process is characterised by a double phase transition (seeing most clearly as two maxima in the dM/dH curves in the bottom-left panel of Fig. 6) indicative of the appearance of magnetisation plateau. Although the plateau is not well-pronounced, *i.e.* the derivative dM/dH remains positive and relatively large between the maxima, one has to remember that the temperature for these measurements was relatively high, 0.5 K . For $T = 2.0 \text{ K}$ (see right-hand panels in Fig. 6), the plateau in the magnetisation disappears. Therefore, it is likely that at the temperatures approaching 0 K the plateau will be much more obvious. The value of the magnetisation on the plateau is about a third of the value observed in higher field. This fact allows to conjecture²³ that the magnetic structure on the plateau is of collinear *up-up-down* type, where on each triangle the two moments are pointing along the applied field and the third moment is antiparallel to them.

For $H \parallel c$ the magnetisation process in SrHo_2O_4 is

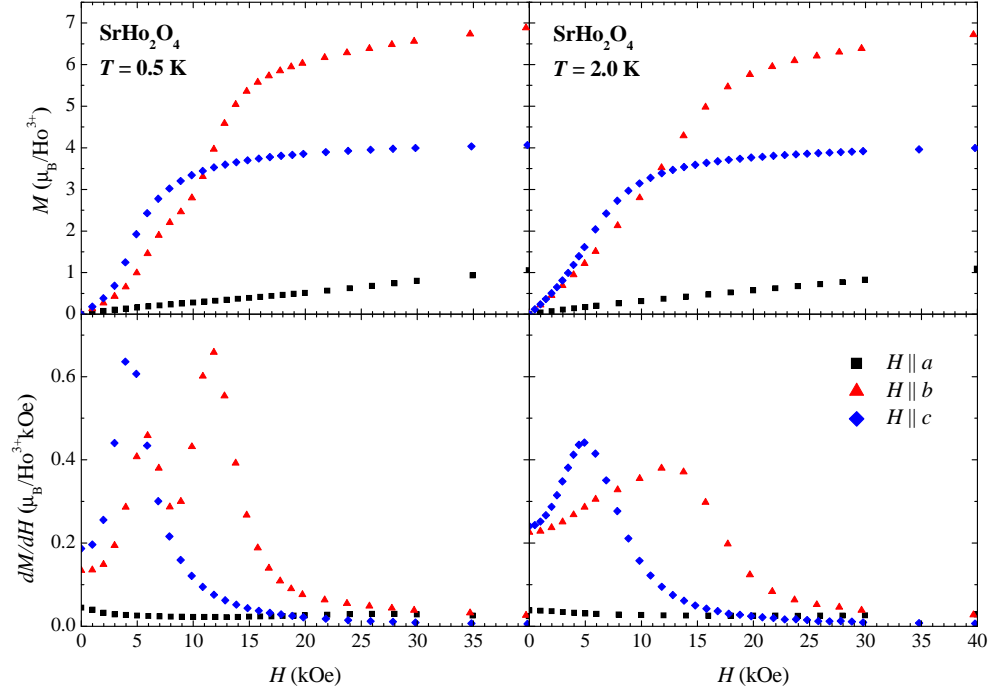


FIG. 6: Field-dependent magnetisation curves (top panels) for SrHo_2O_4 obtained at 0.5 K (left) and 2.0 K (right) in the range of fields 0 to 40 kOe. (Bottom panels) The field derivatives of the magnetisation at 0.5 K (left) and 2.0 K (right). Figure is from Ref. [23].

characterised by a single, relatively sharp phase transition, above which the magnetisation remains practically constant. For $T = 2.0$ K (see right-hand panels in Fig. 6), the plateau in the magnetisation disappears, the maximum in dM/dH for $H \parallel c$ broadens and shifts to slightly higher fields, while the $M(H)$ curve for $H \parallel a$ remains unchanged.

In SrEr_2O_4 and SrDy_2O_4 the field dependence of the magnetisation looks rather similar to what have been observed in SrHo_2O_4 , but the directions of applied field along which the plateaux and sharp single phase transitions appear (as well as the actual values of critical fields) are different. In all three compounds a single and relatively sharp increase in magnetisation is seen for $H \parallel c$, a direction along which the magnetic moments are pointing in the $\mathbf{k} = 0$ structures of SrEr_2O_4 and SrHo_2O_4 . In SrEr_2O_4 the application of field along the a axis results in a magnetisation plateau, while the b axis seems to be a hard magnetisation direction. In SrDy_2O_4 a magnetisation plateau appears for $H \parallel b$, while the a axis seems to be a hard magnetisation direction.

The fact that in all three compounds the observed plateaux in magnetisation appear at approximately a third of the magnetisation saturation values suggests that for the field applied along either the a or b axes the contribution from the $\mathbf{k} = 0$ structures remains rather weak, that is, the magnetic moments in these structures remain pointing along the c axis.

Further insight into the field-induced properties of

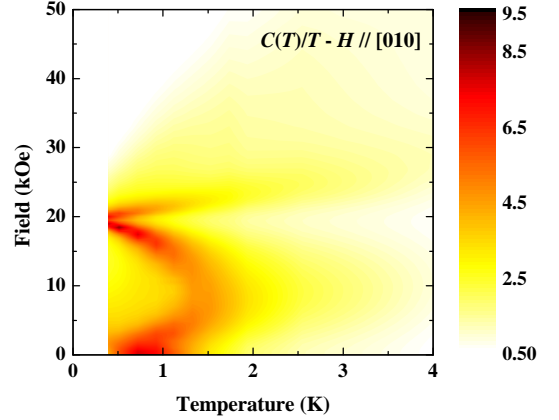


FIG. 7: Magnetic $H - T$ phase diagram of SrDy_2O_4 for $H \parallel [010]$ obtained from the heat capacity measurements. Colour represents the heat capacity divided by temperature in the units of $\text{J}/(\text{mol K}^2)$. Figure is from Ref. [22].

SrDy_2O_4 can be gained from the heat capacity measurements²². Fig. 7 (where the value of the heat capacity divided by temperature is represented by the colour scale shown on the right of the figure) shows a magnetic phase diagram of SrDy_2O_4 obtained by combining the heat capacity field-scans for $H \parallel b$. At the lowest experimentally available temperature of 0.39 K, a sharp double peak at about 20 kOe is the main feature in the $C(H)$ curve.

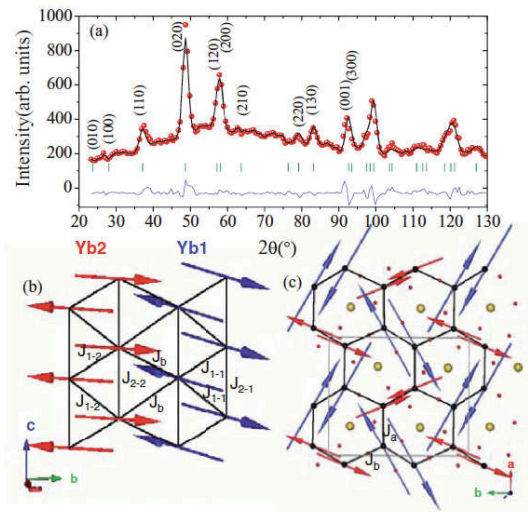


FIG. 8: (a) Magnetic powder pattern of SrYb_2O_4 collected on D7 at 30 mK. The magnetic structure where the arrows represent the Yb^{3+} ions spins (Yb1 blue, Yb2 red) (b) along the zigzag chains and (c) projected onto the ab plane. The Sr^{2+} and O^{2-} ions are represented by yellow and red circles, respectively. Figure is from Ref. [12].

The peaks indicate multiple magnetic field-induced transitions in SrDy_2O_4 for this direction of an applied field, but from the bulk-property measurements alone it is impossible to determine whether any of the field-induced phases are long-range in nature. Therefore further neutron diffraction experiments are required to answer this question. Remarkably for $H \parallel c$ the application of a magnetic field does not result in any features in the $C(H)$ curves sharp enough to be indicative of a phase transition²² which emphasises once again the highly anisotropic nature of the magnetisation process in the SrLn_2O_4 compounds.

IV. FURTHER CONSIDERATIONS

A. Other SrLn_2O_4 compounds

Apart from SrEr_2O_4 , SrHo_2O_4 and SrDy_2O_4 reviewed above, the only other family-member for which the low-temperature properties have been reported is SrYb_2O_4 . Heat capacity measurements¹² revealed a magnetic phase transition to LRO at $T_N = 0.92$ K. Neutron diffraction measurements¹² (see Fig. 8a) showed that the structure is a noncollinear $\mathbf{k} = 0$ antiferromagnet in which the magnetic moments of two inequivalent Yb^{3+} ions lie in the ab plane, but have different moment sizes and directions. Both moments are reduced from the fully ordered moment of Yb^{3+} (see Figs. 8b and 8c). Similarly to what has been observed for other SrLn_2O_4 compounds, the application of a relatively strong field, 140 kOe, along any direction does not result in a recovery of a full moment

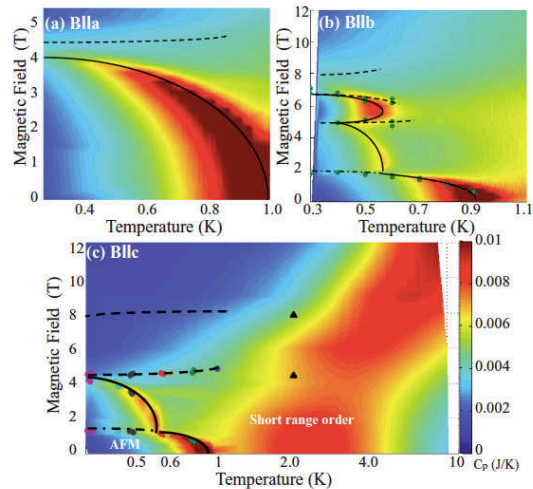


FIG. 9: Magnetic phase diagram of SrYb_2O_4 with magnetic field along (a) a , (b) b , and (c) c axes. The colours indicate the heat capacity in units of J/K . The circles indicate the critical fields extracted from magnetocaloric effect measurements and the triangles the critical fields extracted from magnetisation measurements. Black solid lines show second-order phase transitions. Dash-dot black lines indicate the transition from the AFM phase to a less ordered one. Dashed black lines show metamagnetic crossovers. For the phase diagram along the c axis, above 4.5 T there are just three heat capacity scans at 6, 9, and 12 T, the colours between them result from the interpolation of the data. Below 4.5 T, the data were collected every 0.2 T. The temperature axis is in logarithmic scale. Figure is from Ref. [12].

expected for the Yb^{3+} ions¹².

Very interesting and highly anisotropic magnetic phase diagrams (see Fig. 9) have been reconstructed for SrYb_2O_4 from the magnetocaloric and the magnetisation measurements¹². A large number of transitions and crossovers were found which has been taken as an indication of the presence of metamagnetic phases due to spin-flip and spin-flop processes as well as possible competition between exchange interactions and magnetic anisotropy, however, the exact nature of the field-induced phases in SrYb_2O_4 remains presently unknown.

We have recently started investigations of the magnetic properties of SrGd_2O_4 and from the heat capacity measurements have found²⁵ that the compound undergoes two magnetic transitions at 2.72 and 0.47 K. The initial characterisation of SrGd_2O_4 by Karunadasa *et al.*⁴ missed the higher temperature transition. Since Gd^{3+} is expected to be nearly isotropic, it is quite surprising that the transition temperature of SrGd_2O_4 is much higher than that of the other members of the family. The higher ordering temperature of SrGd_2O_4 is, however, consistent with the properties of structurally similar BaLn_2O_4 family, in which BaGd_2O_4 orders at 2.6 K, while the rest of the compounds do not order down to at least 1.7 K¹³. In the absence of neutron diffraction data the magnetic structure of SrGd_2O_4 remains unknown at present. The

only other established fact about low-temperature properties of SrGd_2O_4 is that it undergoes a field-induced transformation at 20.5 kOe (for $T = 0.48$ K) in a field applied along the c axis²⁵.

It would certainly be interesting to expand the SrLn_2O_4 family and to test the magnetic properties of Tm, Tb, Sm, Nd containing compounds provided that single crystal samples can be prepared.

B. Crystalline electric field effects

From the findings presented above for the SrLn_2O_4 compounds, which vary greatly from one Ln ion to another, it is rather obvious that the low-lying crystalline electric field (CEF) levels must play an important role in the formation of the highly anisotropic magnetic properties. At present the CEF schemes remain unknown and the task of establishing them may not be trivial: there are 8 Ln ions on two distinct crystallographic sites in the unit cell. The symmetry is rather low, therefore the number of CEF levels is expected to be large. Also, the positions of the levels at lower temperature can potentially be influenced by the development of short-range magnetic order. Inelastic neutron scattering (INS) data for SrDy_2O_4 and SrHo_2O_4 have been collected back in 2005 by Kenzelman *et al.*²⁶. The more recent INS results reported for SrHo_2O_4 by Ghosh *et al.*¹¹ are largely in agreement with the previous data. We have also collected further INS data for SrEr_2O_4 ²⁷, but to date neither group have reported any CEF schemes. Moreover, there are further indications²⁸ that the problem could prove to be difficult to solve. An additional motivation for preparing this review was to alert the frustrated magnetism community to the presence of such a challenging, but potentially very important problem.

V. SUMMARY

We conclude this review by listing in Table I the most important magnetic parameters of the SrLn_2O_4 compounds, such as Weiss temperature Θ_W , effective moment p_{eff} in Bohr magnetons μ_B , magnetic ordering temperature T_N as well as indicating the nature of the zero field ground state and the presence of critical fields H_C for different directions of an applied field.

Important pieces of information missing from Table I include the values of the various exchange interactions and details on the magnetic anisotropy in the SrLn_2O_4 compounds. This information which is typically obtained from inelastic neutron scattering experiments is so far unavailable. Only after establishing the absolute values (including signs) and relative strengths of the relevant exchange interactions, as well as details of the magnetic anisotropy, could one classify the SrLn_2O_4 compounds

as a collection of weakly interacting chains of magnetic moments, or as a network of ladders consisting of triangles. Apart from neutron scattering, further Monte Carlo simulations, both direct and reverse, as well as density-functional theory band-structure calculations may play an important role in determining the magnetic interactions.

In SrEr_2O_4 the LRO $\mathbf{k} = 0$ AFM phase (see Fig. 3) in which the magnetic moments point along the c axis appears below 0.75 K while in SrHo_2O_4 a very similar phase appearing below 0.68 K remains short-range ordered down at least 50 mK. Apart from this phase, a SRO quasi one-dimensional AFM component is found in both compounds, but the direction along which the spins are pointing is different - it is parallel to the a axis in SrEr_2O_4 and parallel to the b axis in SrHo_2O_4 . In SrEr_2O_4 the diffuse scattering signal corresponding to the quasi 1D component appears to be much more structured compared to the SrHo_2O_4 , which could be indicative of the importance of further neighbour exchange interactions. In SrYb_2O_4 the magnetic moments are confined to the ab plane (see Figs. 8b and 8c), with the two different Yb^{3+} sites having very different moment sizes and directions¹². No long-range magnetic order has been found in SrDy_2O_4 down to 20 mK. Despite having the weakest magnetic interactions (as demonstrated by the lowest Weiss temperature) SrGd_2O_4 orders at the highest temperature of 2.72 K and undergoes another transition at 0.47 K. This observation suggests an immense importance of the magnetic anisotropy in establishing the ground state of the SrLn_2O_4 compounds and the potential competition between the exchange interactions and the single-ion effects.

For all the SrLn_2O_4 compounds the application of an external magnetic field results in the appearance of complex and highly anisotropic phase diagrams revealing multiple phase transitions, magnetisation plateaux and cross-over regions. The magnetic structure of the field-induced phases remains presently unknown.

We hope that this review will stimulate further research on the magnetic properties of the SrLn_2O_4 and related honeycomb lattice compounds.

VI. ACKNOWLEDGEMENTS

The author is very grateful to G. Balakrishnan, M.R. Lees, D.McK. Paul, N.R. Wilson, T.J. Hayes, O. Young, T.H. Cheffings, P. Manuel, D.D. Khalyavin, D.T. Adroja, F. Demmel, B.D. Rainford, A.R. Wildes, B. Ouladdiaf, L.C. Chapon, S. de Brion, E. Suard, C. Ritter, P.P. Deen, R.J. Mason, A.K.R. Briffa, M.W. Long, J. Mercer, M.L. Plumer, A. Desilets-Benoit, A.D. Bianchi, and D.L. Quintero-Castro for the collaborations on the projects involving the magnetic properties of the SrLn_2O_4 compounds.

Ln	Θ_W , K	p_{eff} , μ_B	T_N , K	Magnetic structure (in zero field)	H_C , kOe
Er	-13.5 ⁴	9.176 ⁴	0.75 ¹⁷	$\mathbf{k} = 0$ LRO AFM (moments $\parallel c$ axis) ¹⁷ & quasi 1D SRO AFM (moments $\parallel a$ axis) ¹⁸	$H \parallel c$: 5.4 (0.5 K) ²³ $H \parallel a$: 2.0 & 12.5 (0.5 K) ²³
Ho	-16.9 ⁴	10.50 ⁴	0.68 ¹⁹	$\mathbf{k} = 0$ SRO AFM (moments $\parallel c$ axis) & quasi 1D SRO AFM (moments $\parallel b$ axis) ²⁰	$H \parallel c$: 4.0 (0.5 K) ²³ $H \parallel b$: 5.9 & 12.0 (0.5 K) ²³
Dy	-22.9 ⁴	10.35 ⁴	<0.02 ²²	only SRO above 0.02 K ²²	$H \parallel b$: 1.6 & 20.3 (0.5 K) ²³ , 20 (0.39 K) ²² $H \parallel c$: 12.0 (0.5 K) ²³
Gd	-9.0 ⁴	8.02 ⁴	0.47 & 2.72 ²⁵	unknown	$H \parallel c$: 20.5 (0.48 K) ²⁵
Yb	-99.4 ⁴	4.348 ⁴	0.92 ¹²	noncollinear $\mathbf{k} = 0$ AFM with different moment sizes and directions ¹²	$H \parallel a$: 45 (1.0 K) ¹² $H \parallel b$: 15 & 60 (0.6 K) ¹² $H \parallel c$: 11 & 45 (0.6 K) ¹²

TABLE I: Summary of the magnetic properties of the SrLn_2O_4 compounds. Θ_W is Weiss temperature and p_{eff} is an effective magnetic moment. Both parameters were determined from the higher-temperature susceptibility measurements. For the transitions fields H_C the corresponding measurement temperatures are indicated in the brackets.

-
- ¹ A.P. Ramirez, Annu. Rev. Mater. Sci. **24**, 453 (1994); M.F. Collins and O.A. Petrenko, Can. J. Phys. **75**, 605 (1997); S.T. Bramwell and M.J.P. Gingras, Science **294**, 1495 (2001); H.T. Diep (ed.), *Frustrated Spin Systems*, World Scientific, Singapore, (2005); J.S. Gardner, M.J.P. Gingras and J.E. Greedan, Rev. Mod. Phys. **82**, 53 (2010); C. Lacroix, P. Mendels and F. Mila (ed.), *Introduction to Frustrated Magnetism*, Springer Series in Solid-State Sciences **164**, (2011).
- ² B.F. Decker and J.S. Kasper, Acta Cryst. **10**, 332 (1957).
- ³ L. M. Lopato and A. E. Kushchevskii, Ukr. Khim. Zh. **39**, 7 (1973).
- ⁴ H. Karunadasa, Q. Huang, B.G. Ueland, J.W. Lynn, P. Schiffer, K.A. Regan, and R.J. Cava, Phys. Rev. B **71**, 144414 (2005).
- ⁵ F. Damay, C. Martin, V. Hardy, A. Maignan, G. Andre, K. Knight, S.R. Giblin, and L.C. Chapon, Phys. Rev. B **81**, 214405 (2010); F. Damay, C. Martin, V. Hardy, A. Maignan, C. Stock, and S. Petit, Phys. Rev. B **84**, 020402 (2011).
- ⁶ S. Das, A. Niaz, Y. Mudryk, V.K. Pecharsky, and D.C. Johnston, Phys. Rev. B **81**, 104432 (2010).
- ⁷ F. Ye, S. Chi, H. Cao, B.C. Chakoumakos, J.A. Fernandez-Baca, R. Custelcean, T.F. Qi, O.B. Korneta, and G. Cao, Phys. Rev. B **85**, 180403 (2012).
- ⁸ J. Chaloupka, G. Jackeli, and G. Khaliullin, Phys. Rev. Lett. **110**, 097204 (2013).
- ⁹ A. Yoshimori, J. Phys. Soc. Japan **14**, 807 (1959).
- ¹⁰ G. Balakrishnan, T.J. Hayes, O.A. Petrenko and D. McK. Paul, J. Phys.: Cond. Matter **21**, 012202 (2009).
- ¹¹ S. Ghosh, H.D. Zhou, L. Balicas, S. Hill, J.S. Gardner, Y. Qiu, and C.R. Wiebe, J. Phys.: Cond. Matter **23**, 164203 (2011).
- ¹² D.L. Quintero-Castro, B. Lake, M. Reehuis, A. Niazi, H. Ryll, A.T.M.N. Islam, T. Fennell, S.A.J. Kimber, B. Klemke, J. Ollivier, V. Garcia Sakai, P.P. Deen, and H. Mutka, Phys. Rev. B **86**, 064203 (2012).
- ¹³ Y. Doi, W. Nakamori, and Y. Hinatsu, J. Phys.: Cond. Matter **18**, 333 (2006).
- ¹⁴ K. Hirose, Y. Doi, and Y. Hinatsu, J. Solid State Chem. **182**, 1624 (2009).
- ¹⁵ O. Ofer, J. Sugiyama, J.H. Brewer, E.J. Ansaldo, M. Månsson, K.H. Chow, K. Kamazawa, Y. Doi, and Y. Hinatsu, Phys. Rev. B **84**, 054428 (2011).
- ¹⁶ Y. Misawa, Y. Doi, and Y. Hinatsu, J. Cer. Soc. Japan, **117**, 85 (2009).
- ¹⁷ O.A. Petrenko, G. Balakrishnan, N.R. Wilson, S. de Brion, E. Suard and L.C. Chapon, Phys. Rev. B **78**, 184410 (2008).
- ¹⁸ T.J. Hayes, G. Balakrishnan, P.P. Deen, P. Manuel, L.C. Chapon and O.A. Petrenko, Phys. Rev. B **84**, 174435 (2011).
- ¹⁹ O. Young, L.C. Chapon and O.A. Petrenko, J. Phys.: Conf. Series **391**, 012081 (2012).
- ²⁰ O. Young, A.R. Wildes, P. Manuel, B. Ouladdiaf, D.D. Khalyavin, G. Balakrishnan and O.A. Petrenko, Phys. Rev. B **88**, 024411 (2013).
- ²¹ J.R. Stewart, P.P. Deen, K.H. Andersen, H. Schober, J.-F. Barthemy, J.M. Hillier, A.P. Murani, T. Hayes, and B. Lindenau, J. Appl. Crystallogr. **42**, 69 (2009).
- ²² T.H. Cheffings, M.R. Lees, G. Balakrishnan and O.A. Petrenko, J. Phys.: Cond. Matter **25**, 256001 (2013).
- ²³ T.J. Hayes, O. Young, G. Balakrishnan, and O.A. Petrenko, J. Phys. Soc. Japan **81**, 024708 (2012).
- ²⁴ O.A. Petrenko, L.C. Chapon, and T.J. Hayes *ILL Exp. Rep.* 5-31-1695.
- ²⁵ O. Young, G. Balakrishnan and O.A. Petrenko, unpublished (2013).
- ²⁶ M. Kenzelmann and B. Rosendahl Hansen, ISIS experimental report 510364.
- ²⁷ O.A. Petrenko, T.J. Hayes and F. Demmel: ISIS experimental report 920327.
- ²⁸ A. Desilets-Benoit, Thesis, Universite de Montreal (2010).